

The Chandigarh variable energy cyclotron

I M GOVIL and H S HANS

Department of Physics, Panjab University, Chandigarh 160 014

MS received 16 November 1979; revised 26 May 1980

Abstract. The characteristics and performance of the variable energy cyclotron at Chandigarh have been described. The machine operates for protons at 1 to 5 MeV, for deuterons at 4 MeV, for alphas from 1 to 2 MeV and 7 to 8 MeV, and He^{3++} upto 11 MeV. The resolved beams of different particles from 30 nA to 1 μA have been obtained at the target with a resolution of about 30 keV. The magnetic field and the beam profile in the chamber are discussed. Various gamma-ray and charged particle spectra are given to indicate the performance of the accelerator.

Keywords. Classical cyclotron; variable energy; protons; deuterons; alphas; He^{3++}

1. Introduction

The variable energy cyclotron at Chandigarh has now been functioning for the last three years with resolved beams of protons, deuterons, alphas and He^{3++} at the main target chamber. The beams of protons of energy from 1 to 5 MeV, deuterons for 4 MeV, alphas from 1 to 2 MeV and from 7 to 8 MeV, and He^{3++} upto 11 MeV have been obtained at the target. This paper describes the various features of this cyclotron and the characteristics of the accelerated particles.

2. Main features

This machine at Chandigarh is adapted and built out of the components of the variable energy cyclotron at the University of Rochester, Rochester, New York, USA, originally used by Fulbright (1959). It is a single Dee classical cyclotron with arrangement for variable frequencies from 10 to 20 MHz, and a main magnetic field upto a maximum of 14 k Gauss. This permits the variability of the energy of the various accelerated ions. The layout plan of the whole set-up is shown in figure 1.

All the operations of the machine are controlled from a control desk. It is possible to maintain a pressure of 5×10^{-6} mm Hg in the whole vacuum system. A total power of 110 kW is required when the machine is fully operative with all the accessories.

The operational characteristics and the general features of the cyclotron have earlier been described by the authors (Govil & Hans 1976).

3. The main magnet

The lids of the main chamber form the tips of the polepieces of the main magnet

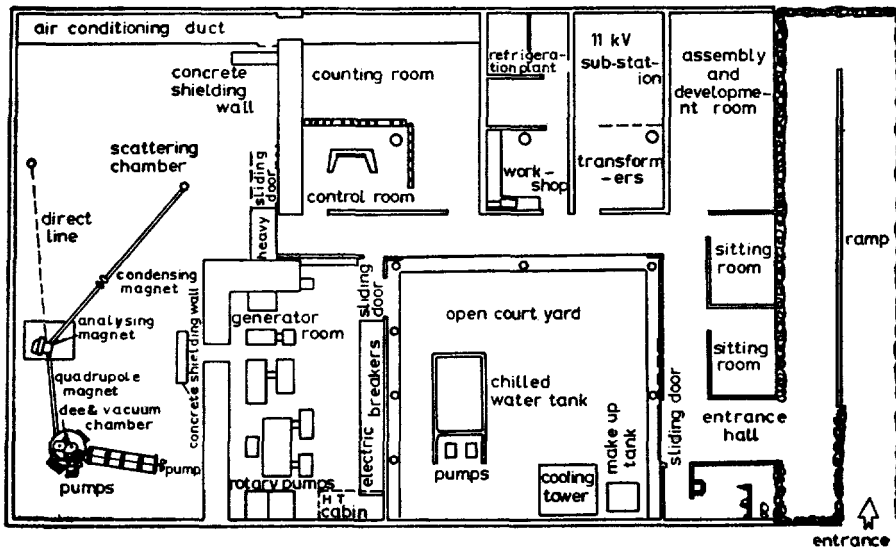


Figure 1. General layout plan of the cyclotron laboratory.

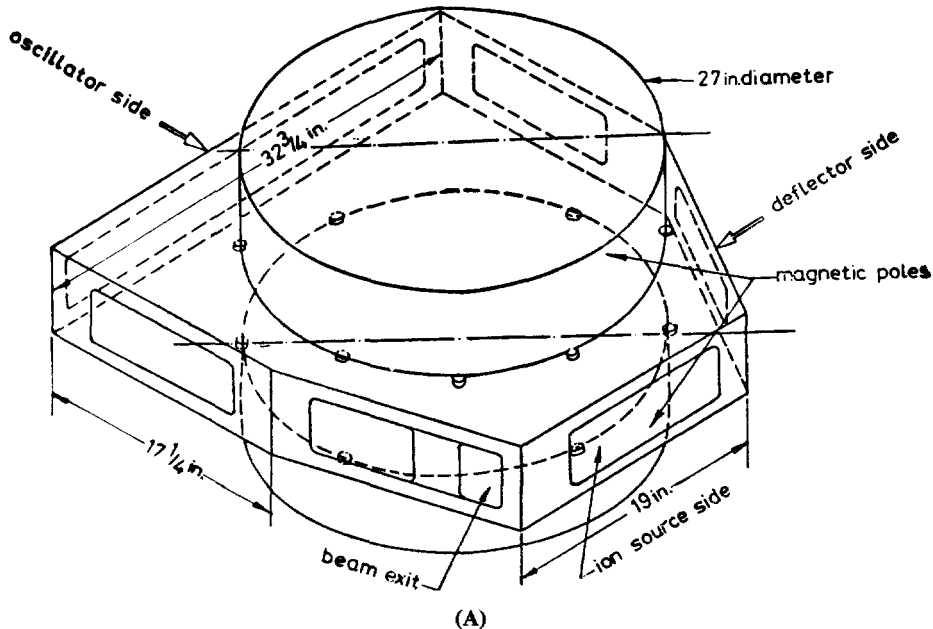
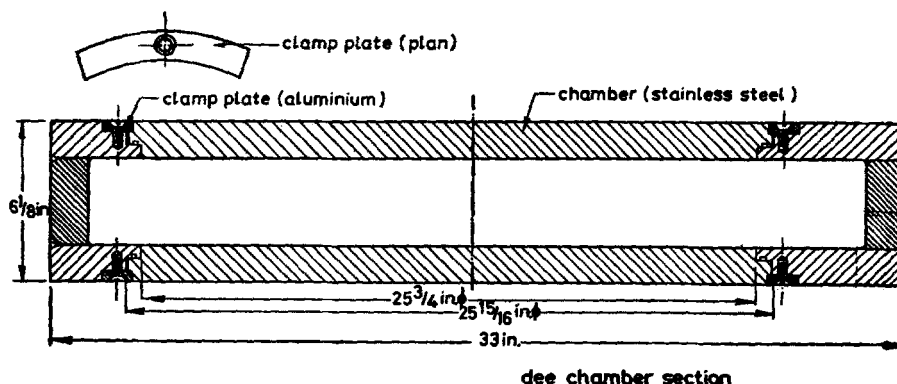


Figure 2a. Configuration of Dee chamber with the pole pieces. The spacers are also shown.

(67.5 cm in diameter) and serve as the main magnetic field as well as the seal to the vacuum as shown in figures 2a, b. The magnet has four current-carrying coils—two on each side, each carrying a maximum current of 100 A, at 100V. The current is supplied by a DC generator whose output is stabilised by a feedback system, as shown in figure 3 by using the shunt in series of the coils and a DC amplifier. The stability of the magnetic fields is better than 1 in 10^5 which was indicated by the stability of the resonance signal of the NMR probe on the oscilloscope.



(B)

Figure 2b. Profile of the clamp plate attached to the chamber.

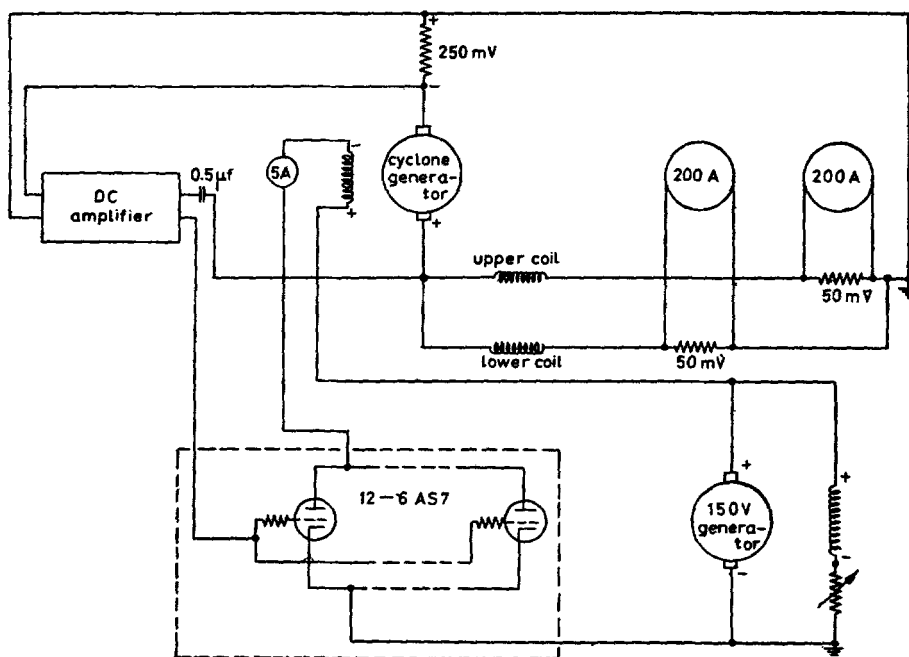


Figure 3. Circuitry used for stabilising the voltage of the DC generator for the main magnet and the analyser.

The mapping of the profile of the magnetic fields is accomplished by using a search coil and a fluxmeter with a sensitivity of relative measurement upto 1 Gauss. However, it must be mentioned that the mapping is not very accurate, as the profile of the magnetic field was measured by a fluxmeter, with respect to the field at the centre. The absolute value of the field at centre, however, was measured by an NMR probe with much better accuracy. The radial fall-off of the field is shown in figure 4a. The field index

$$\eta = \left(\frac{-dB}{B} \right) \left/ \left(\frac{dr}{r} \right) \right.$$

varies from zero at the centre to 0.1 at the extraction radius of 27.5 cm. It is thus a weak focussing machine. The azimuthal variation of the magnetic field at different radii is shown in figure 4b. The pole fields are so aligned that the contribution of the first harmonic is less than 10 Gauss upto the extraction radius as shown in figure 4c. Therefore no appreciable shift in the beam centre was noticed.

4. The oscillator

The oscillator is driven by a RCA 5771 tube with a dissipation power of 25 kVA and a water cooled anode as shown in figure 5. A cavity, 250 cm long and 65 cm outer diameter with the Dee stem of 7.5 cm diameter forms the tank circuit of the oscillator tube. This is coupled to the tube by filament leads through a coupling cylinder, 25 cm in diameter. The shorting bar controls the frequency of the oscillator by providing a terminated line, the termination being provided by the plate, which connects the stem of the cavity with the outer cylinder. The oscillator operates in $\lambda/4$ mode. The high Q of the oscillator circuits (≈ 1000) takes care of the stability of the frequency and the Dee voltage. The performance of the oscillator greatly improved when the Dee cavity was directly coupled with the main accelerating chamber; in the original design this connection was provided only by a press contact which used to create excessive local heating.

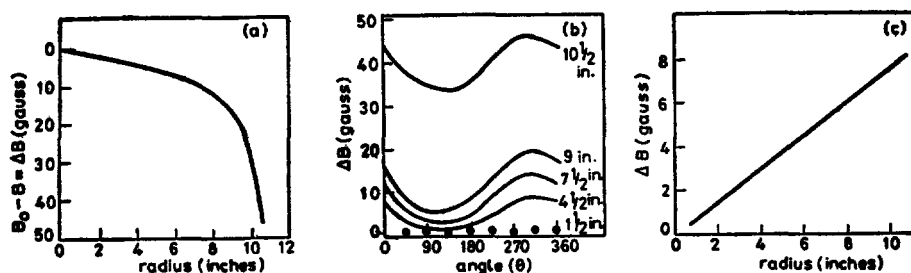


Figure 4. Variation of the magnetic field of the main magnet in the chamber.

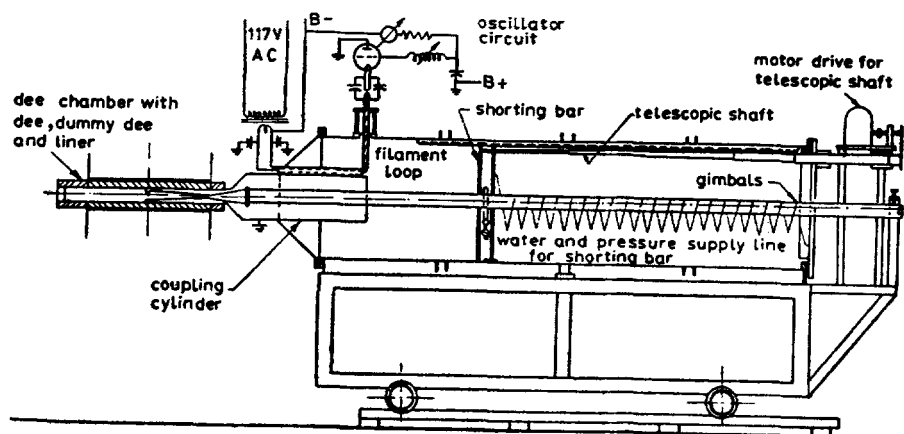


Figure 5. Coupling of the oscillator cavity with Dee.

5. The ion source

The machine was provided with a hooded arc ion source whose physical design was somewhat modified by providing an anticathode at the head for better performance and flexibility of movement. Figure 6 illustrates the final design of the ion source. The ion source is provided with a remote control arrangement for movement of the filaments in the two perpendicular directions. The chimney of the ion source may be moved in x - y - z directions to place the plasma exit hole at a desired position. This is needed to maximise the output current. The output current was found to be quite sensitive to the inclination and position of the ion-source with respect to Dee. The filament of the ion source can be replaced without disturbing the vacuum. The gas flow is controlled by two Edward's needle valves. The power (6.3 V, 300 A) to the filament of the ion source, which was originally provided by a DC motor generator set, has now been replaced by a DC power supply of 6.5 V and 300A.

6. The deflector

The deflector is of a simple electrostatic type with provision for a maximum DC voltage of about 70 kV. The deflector blade with the oil-cooling arrangement is made of copper, and the septum is made of very thin tungsten plate. The positions of the blade and the septum may be controlled remotely from the control desk; this is needed for optimising the extraction of the beam from the deflector. Figure 7a shows the construction and the details of the cooling of the deflector. The septum is kept at ground potential while high voltage is applied on the blade which is made of hollow copper conductor. The blade of the deflector is cooled by circulating the mixture of transformer oil + CCl_4 (ratio 1:2) using a centrifugal pump. The heat of the oil is removed by circulating chilled water as shown in figure 7b.

7. Vacuum system

The vacuum inside the machine is created by four 15 cm and one 23 cm diffusion pump. The fore-vacuum to diffusion pumps is provided by a kinney rotary pump. The addition of the diffusion pump to the oscillator cavity helped to improve the vacuum in the cavity by a factor of two when compared to the Rochester set-up. This

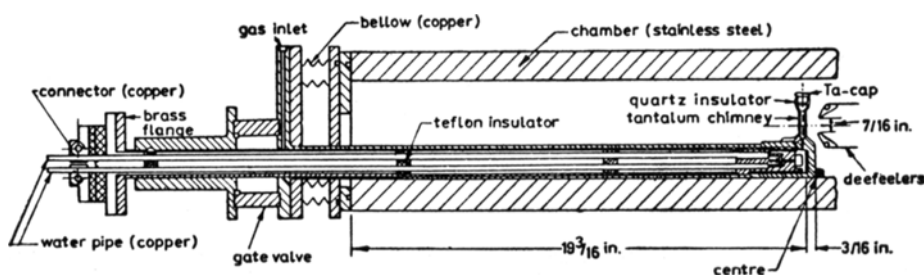
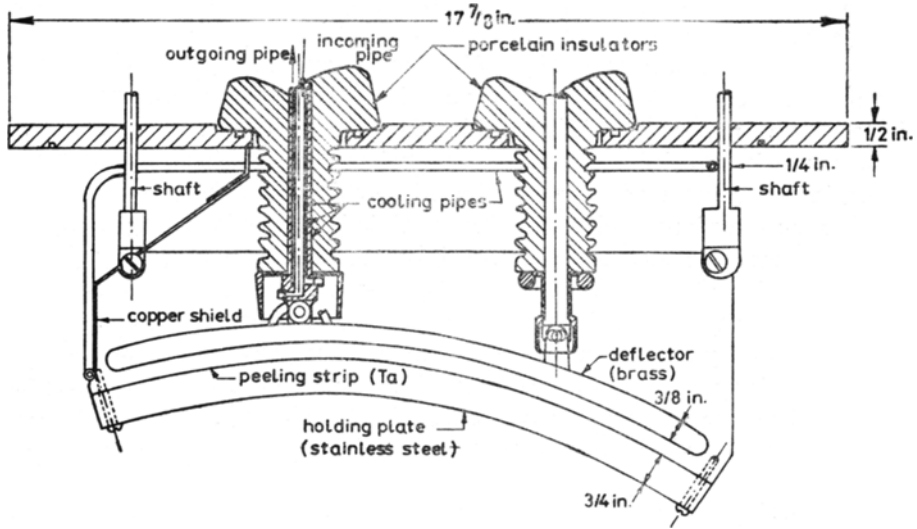
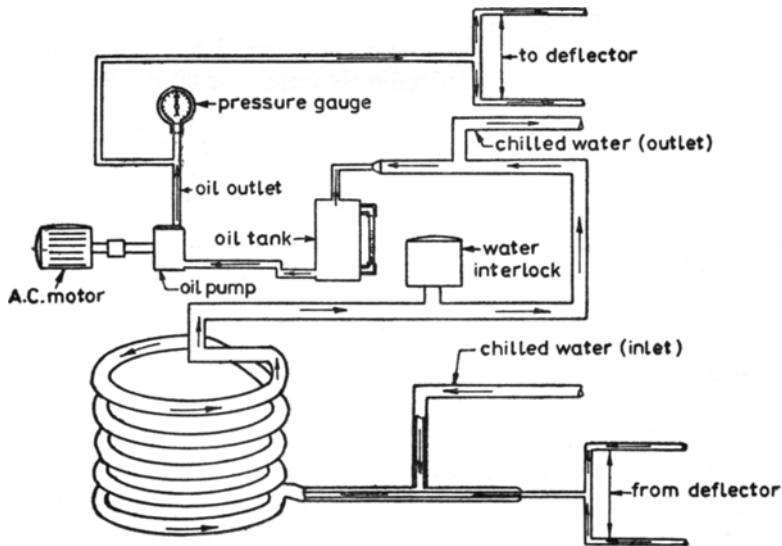


Figure 6. Ion-source assembly and the chimney.



(A)



(B)

Figure 7 a. Deflector showing the insulation and cooling.
b. Cooling system of the deflector

increased the stability of the oscillator many times. The position of some of these pumps is shown in figure 8 (plate 1), which also includes the oscillator cavity.

8. The control system

The various power points in the cyclotron are interlocked with each other, and with various cooling and shielding devices to ensure the safety of the various components,

and of the personnel. Figure 9 (plate 2) shows one of the several panels of relays used for such interconnections.

9. Beam characteristics

Figure 10 shows the variation of the typical beam currents of the various ions at different radii in the main Dee chamber. In runs under the most optimised conditions, we have recently obtained internal beams of protons upto $100 \mu\text{A}$ at 20 cm radius and upto $30 \mu\text{A}$ at full radius. The currents for He^{4++} and He^{3++} are down by a factor of 10 compared to the protons. Table 1 shows the typical extracted beam of different particles at different positions from the deflector upto the target chamber along with its resolution. The behaviour of the He^{3++} ions is similar to that of alpha particles. It is possible to transport the proton beam after the deflector with 50% efficiency, while the alpha-beam drops to about 10%. This is partly due to the poor vacuum in

Table 1. The beam currents at different positions

Particles	Internal beam at 28 cm	After deflector	Before analyser	After analyser
Protons	$9 \mu\text{A}$	$5 \mu\text{A}$	$3 \mu\text{A}$	$1.5 \mu\text{A}$
Deuterons	$2 \mu\text{A}$	$1 \mu\text{A}$	800 nA	300 nA
Alphas	$2 \mu\text{A}$	800 nA	500 nA	200 nA
He^3	$3 \mu\text{A}$	$1.5 \mu\text{A}$	600 nA	100 nA

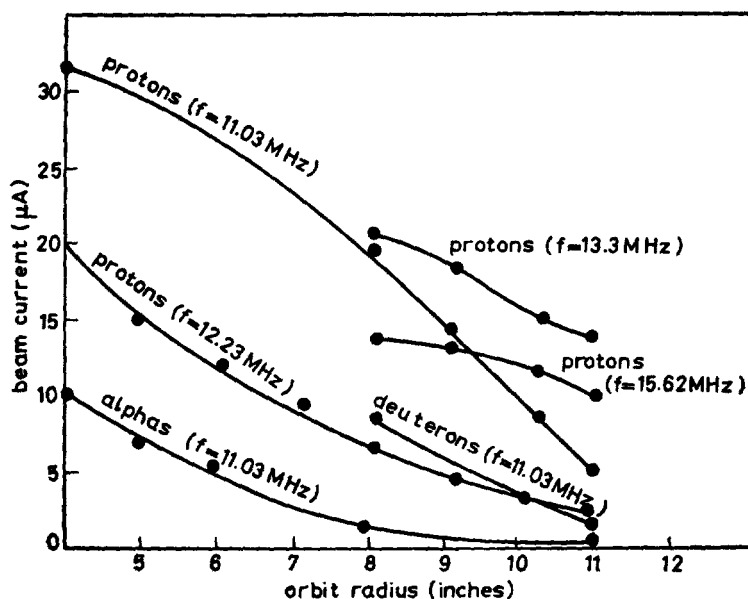


Figure 10. Variation of the internal beam currents inside the chamber.

the beam line and partly to the mixture of other molecular ions with the He^4 beam. Also because of the slits in the beam line the vacuum in the beam line is somewhat impaired. The vacuum in the beam line has been improved by providing differential pumping at different stages and in the target chamber and therefore the transport efficiency of He^{4++} beam has now been increased to 25%.

Apart from the general set-up, the major effort in obtaining the maximum internal beam consisted of (i) alignment of the plasma exit of the chimney of the ion-source, (ii) the alignment of the pole-pieces and the chamber (iii) the alignment of the position of the blade and septum of the deflector, and (iv) proper positioning of the slits and the analyser magnet with respect to the quadrupole lenses in the path of the beam. These efforts took several months before a successful beam for protons was available. For other particles, the filament current, the gas pressure and the arc voltage had to be optimised to get the proper beam, say for alphas, deuterons and He^{3++} ions.

Figures 11 and 12 show the gamma-ray spectra taken with protons and He^{3++} as projectiles on the ^{27}Al target. These two spectra show that there is no appreciable contribution from the background and all the gamma-rays can be attributed to reactions from aluminium. Figure 13 shows the background spectrum for protons, when the beam was stopped behind the shielding wall by a stopper with the proton current for a typical run. It shows that the beam in the main machine does not contribute appreciably to the background. All these spectra were taken at 90° to

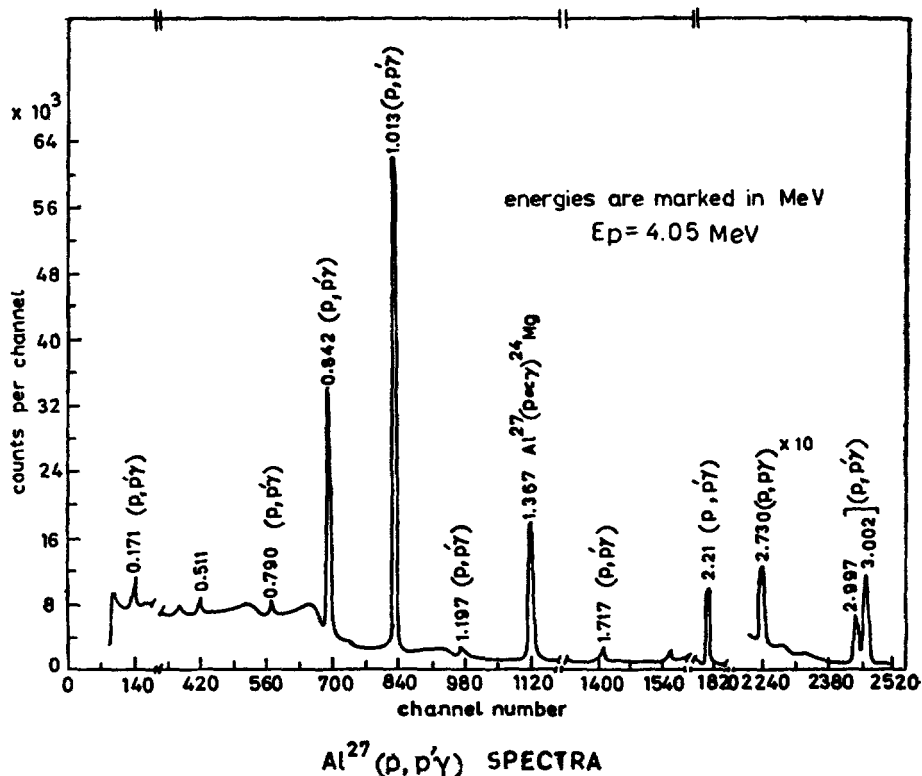


Figure 11. Typical gamma rays spectra due to $^{27}\text{Al} (p, p' \gamma)$ at $E_p = 4.05$ MeV.

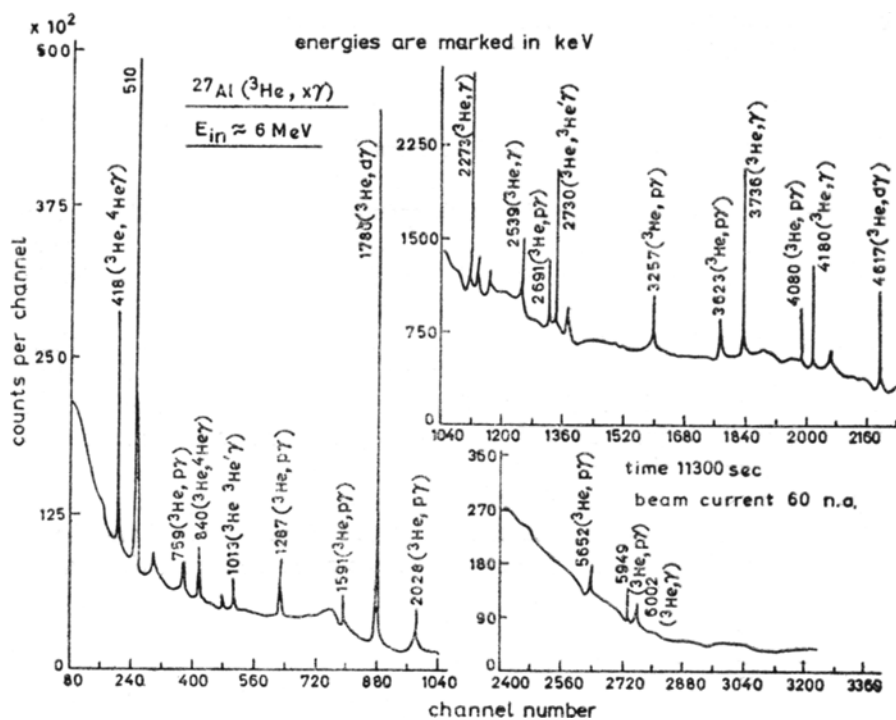


Figure 12. Typical gamma rays spectra due to ^{27}Al (He^3 , $X\gamma$).

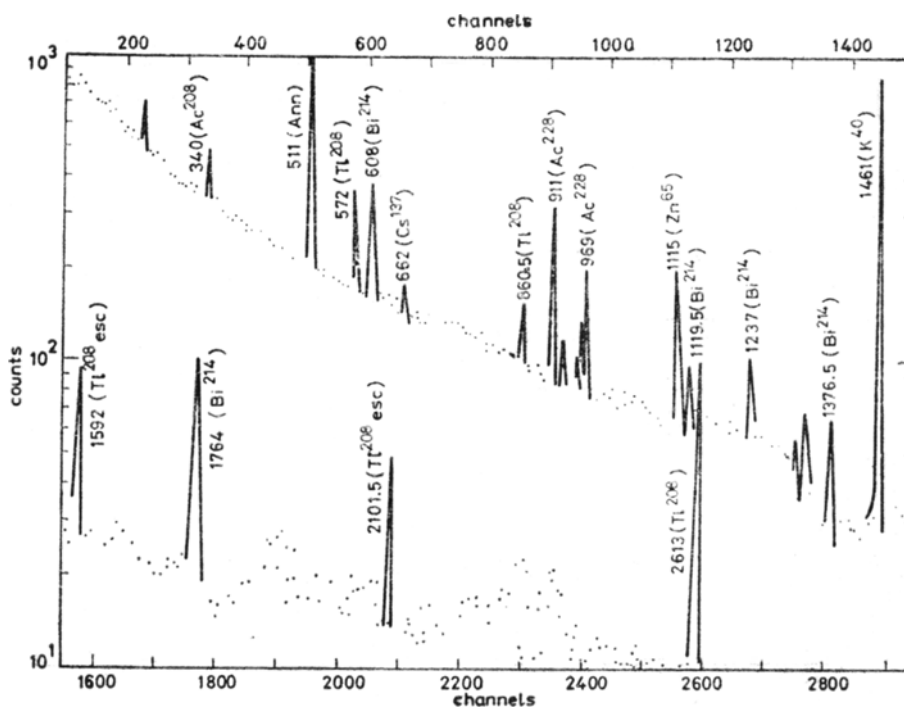


Figure 13. Background gamma spectrum at $E_p = 4.05$ MeV.

the beam direction with the help of 50 cc Ge(Li) detector to avoid broadening of the peaks due to Doppler shift.

10. Energy calibration and resolution of the beam

Figures 14 and 15 show the charged particle spectra arising from the Al target when protons of 3.69 MeV, and alphas of 7.8 MeV were incident. The thickness of the target was 5 keV for protons and 30 keV for alpha particles. The peaks due to inelastic scattering of protons and α -particles are clearly identified. From this, one obtains a beam resolution of 30 keV for protons and 50 keV for alpha particles.

Figure 16 shows the back-scattered proton spectra with bismuth-implanted silicon crystal. One can get an idea of the resolution of the beam from the width of the bismuth peak, which is about 30 keV. These spectra show that the machine can be used for channelling purposes.

Energy calibration of the beam in the cyclotron was affected by two methods *viz.* (i) by measuring the cyclotron resonance frequency; the magnetic field and the radius of the extractions of the beam. The energy can be calculated from the equation

$$E = \frac{q^2}{m} B^2 R^2,$$

where q is the charge of the ions, m the mass of the ion, B the magnetic field and R is the radius of extractions. This is only a rough estimate. For a more accurate

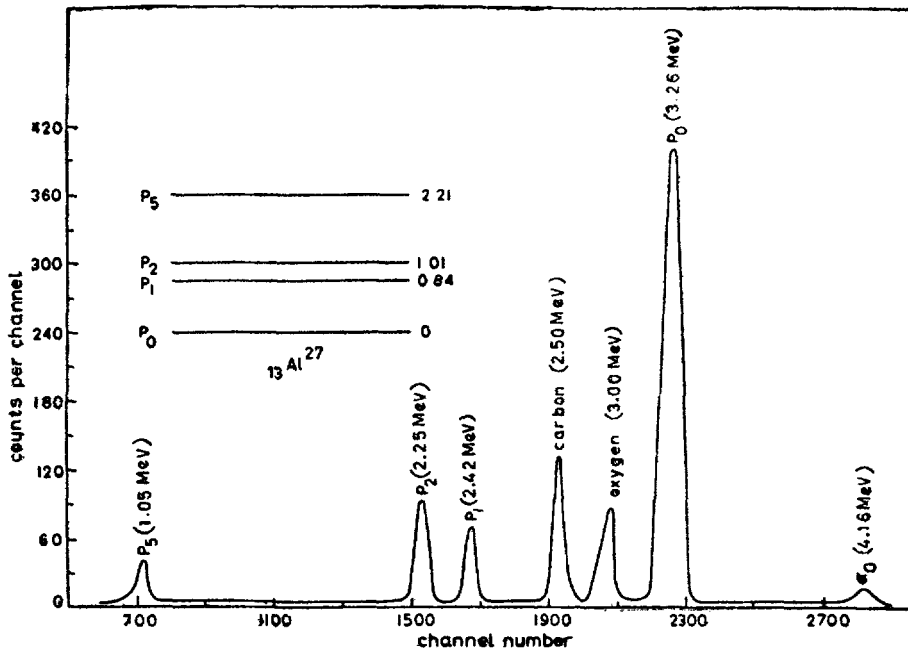


Figure 14. Proton spectrum from ^{27}Al ($p, p' \gamma$).

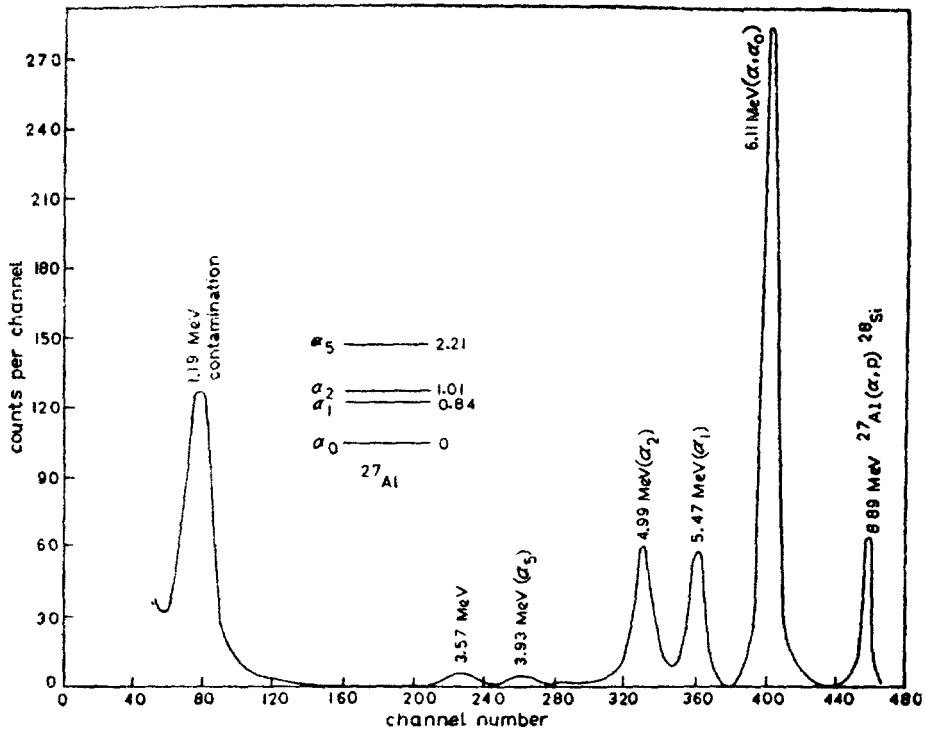


Figure 15. Alpha spectrum from $^{27}\text{Al}(\alpha, \alpha \gamma)$.

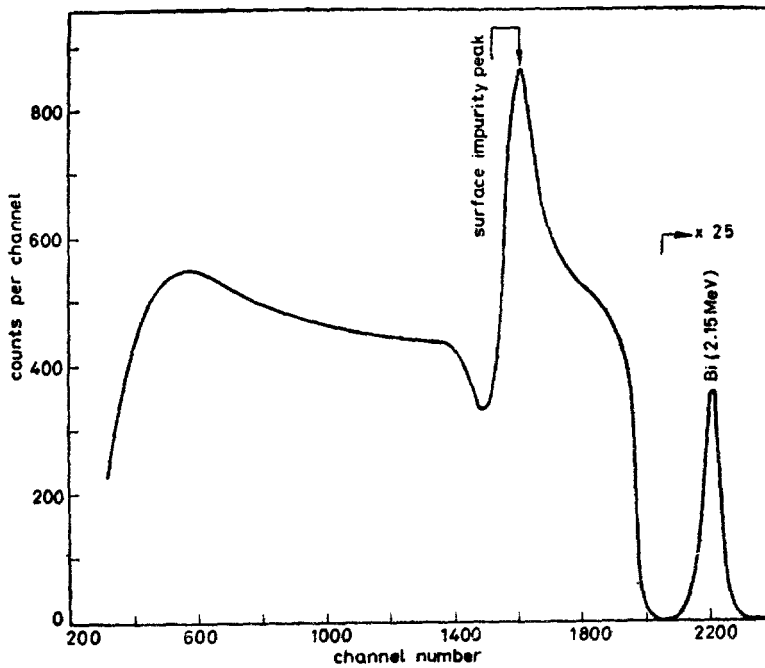


Figure 16. Proton spectrum back-scattered from the thick (Si+Bi) crystal at $E_p = 2.48$ MeV.

measurement, we adopted the following procedure (ii) the beam of protons of a fixed energy is allowed to be backscattered from Al foil; and the charged particle spectrum of the elastically scattered protons (figure 14) is detected by a surface barrier-charged particle detector ($50 \text{ mm}^2 \times 30$), which was sufficiently thick to stop all the particles. The detector was first calibrated using standard α -sources of ^{241}Am and ^{239}Pu . The energy of the elastically scattered peak was obtained from the calibration of the detector, from which the energy of the incident proton beam could be calculated from the kinematics. The difference of the elastically and inelastically scattered peaks also provided another check for the energy calibrations. The resolution of the beam is obtained from the width of the elastically scattered peak.

11. Experiments with the machine

The Chandigarh variable energy cyclotron is now working satisfactorily and is capable of being used for studies with gamma-rays or charged particles. At present three types of experiments are being carried out; these are described below.

(i) In-beam spectroscopy using proton and He^A induced reactions

In these experiments, we have studied the angular distribution of resulting γ -rays from the excited nuclei formed by $(pp' \gamma)$, $(p, n\gamma)$, (p, γ) reactions and similarly with alphas by $(\alpha, p\gamma)$, $(\alpha, n\gamma)$ and $(\alpha\alpha, \gamma)$ reactions.

We have also measured the Doppler shifts in the energy peaks at different angles

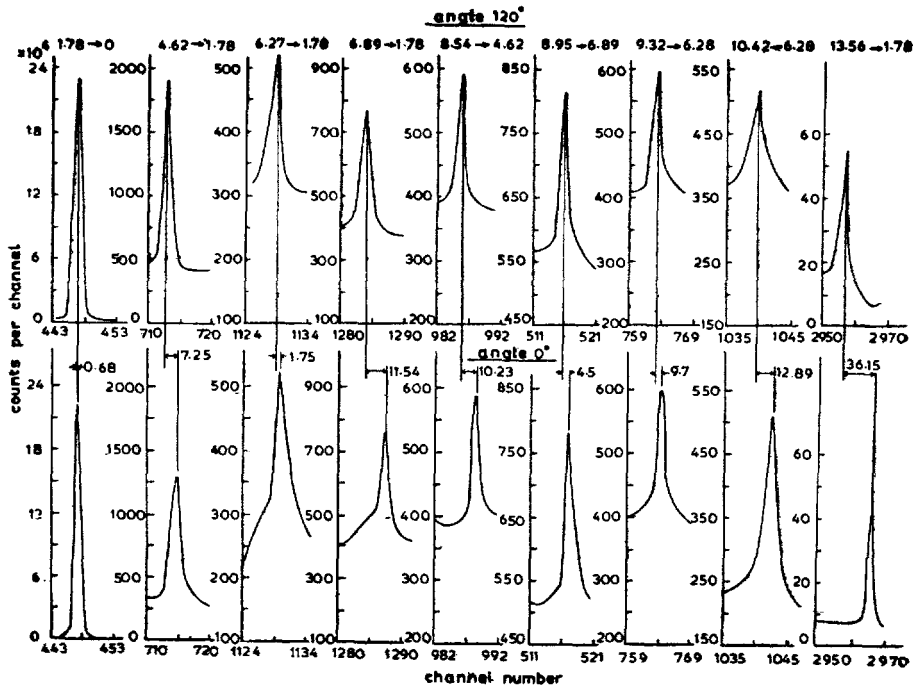


Figure 17. Doppler shift of the gamma-rays spectra from ^{27}Al (p, γ) reaction at $E_p = 2.03 \text{ MeV}$.

in $^{27}\text{Al} (p, \gamma) ^{28}\text{Si}$ reaction, which gives the life-time of the levels using the DSAM techniques. Figure 17 shows typical shifts obtained from $^{27}\text{Al} (p, \gamma)$ reactions. The measurements of shift of a few keV upto 11.8 MeV shows the stability and reliability of the experimental set-up. Many other nuclei have been studied.

(ii) *Coulomb excitation*

The phenomena of Coulomb excitation takes place when protons or α -particles interact with the target nucleus; with the energy lower than the Coulomb barrier.

Many cases of Coulomb excitation have been studied using protons as projectiles. Figure 18 gives the typical excitation function of some of the levels of ^{197}Au , by Coulomb excitation with protons, along with the theoretically expected values. Coulomb excitation on many nuclei have been studied.

(iii) *Shortlived radio isotopes using the cyclotron*

The shortlived isotopes have been produced using the proton and He^4 beam of the machine. A typical case is that of ^{63}Zn , produced by $^{63}\text{Cu} (p, n) ^{63}\text{Zn}$ at 4.5 MeV of proton energy.

Besides the above mentioned experiments, many workers in our laboratory and outside, have shown interest in this machine for other experiments, which may be broadly categorised as follows.

(i) Study of reaction mechanism in He^3 and deuteron-induced reactions, especially in the sub-Coulomb region.

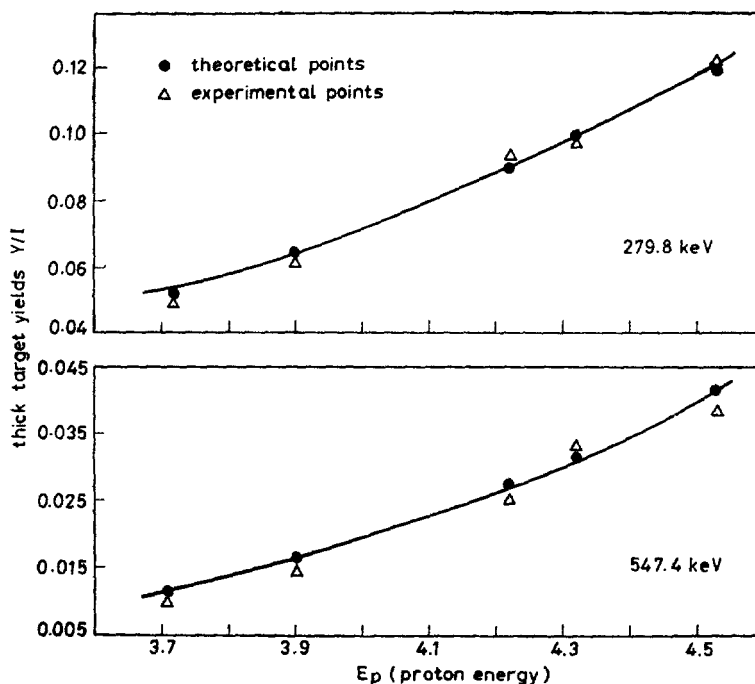


Figure 18. Excitation functions of the reaction $(p, p' \gamma)$, and its comparison with theoretical values based on Coulomb excitation.

(ii) Study of nuclear spectroscopy through He^3 and deuteron-induced reactions. These studies will involve measuring both particles spectra and gamma-rays.

(iii) Nucleo-solid state experiments, for example, hyperfine interactions through

- (a) perturbed angular distribution
- (b) channelling studies
- (c) studies of radiation damages

(iv) proton-induced x-rays for non-destructive analysis.

Some of these experiments are already being planned.

The authors wish to thank the University Grants Commission, the Department of Atomic Energy and the Panjab University for providing funds and facilities for the completion of the project. Our technical staff, Messrs Tej Lal Sharma, Sarmukh Singh, Bishamber Dass and Zora Singh, working under the supervision of Mr S R Bahadur, deserve our special thanks for their devoted efforts in setting up, testing and maintenance of the machine. The authors also thank Drs T S Cheema and B K Arora and Messrs V K Mittal, K P Singh and D K Avasthi for assistance in various measurements. Special thanks are due to Mr Gulzar Singh who helped us to test the various components in the initial stages.

Last, but most importantly, the authors thank Prof. H W Fulbright, Department of Physics, Rochester University, Rochester, New York, USA for transfer of the components of the machine and also for personally helping in introducing improvements in the machine when he was in India for a few weeks in 1977. His help with the chamber for the analysing magnet, which he prepared with personal care, is thankfully acknowledged. Our sincere thanks are due to Mr W B Powell of the University of Birmingham for help in extracting the beam in the initial stages in 1974-75.

References

- Fulbright H W 1959 *Sector focussed cyclotrons* Proc. Conf., Sea Island, Georgia, ed. F T Howard (Washington DC: Natl. Acad. Sci.) p. 174
- Govil I M & Hans H S 1976 *Radiation physics* Proc. National Symp. (Mysore: Mysore University) Vol. 26, p. 23
- Govil I M & Hans H S 1976 *Phys. News (India)* 7 48
- Hans H S 1976 *Few body problems in nuclear and particle physics* ed. A N Mitra *et al* (New York: North Holland) 7 454

Plate 1

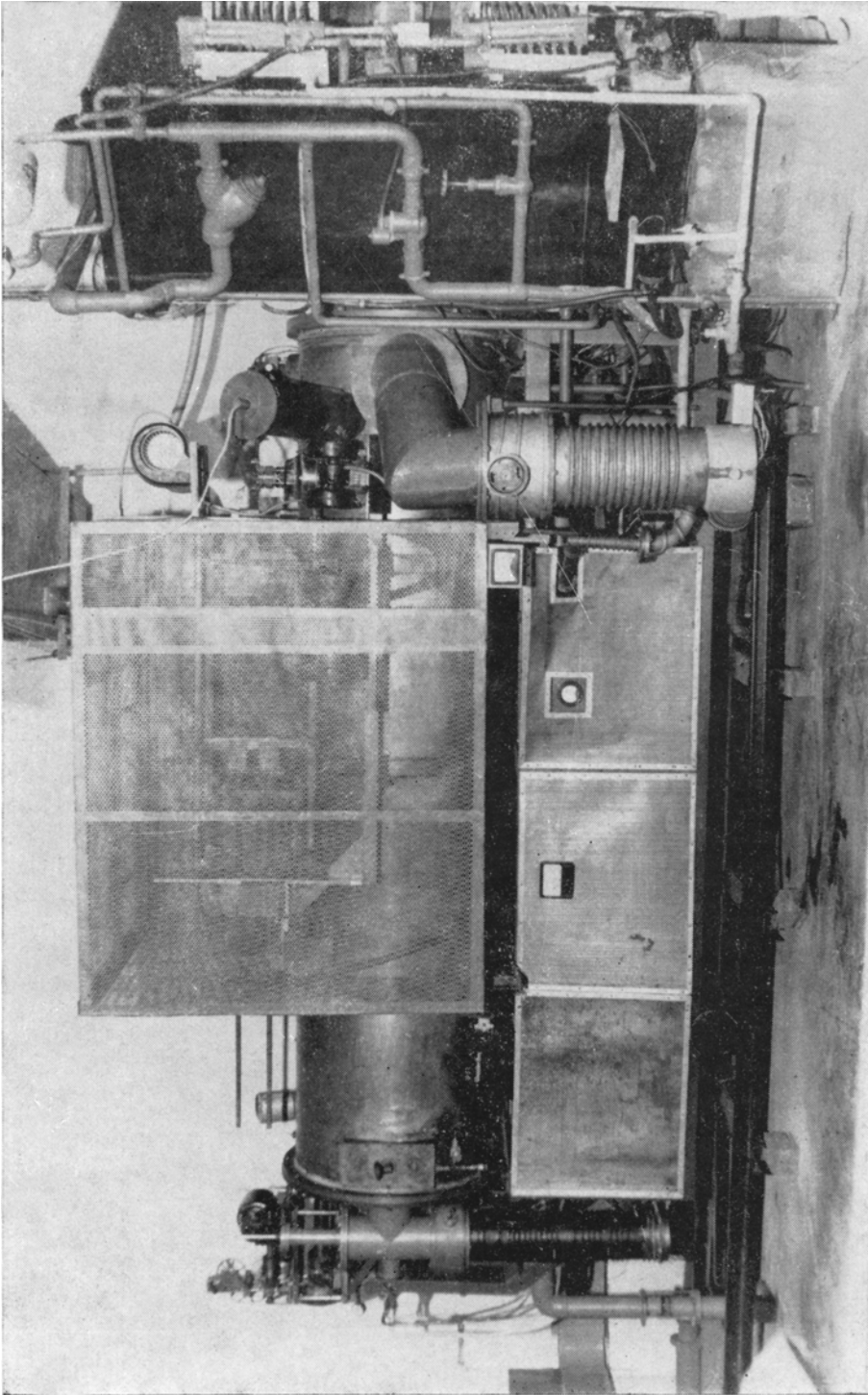


Figure 8. Plate showing the diffusion pumps and the oscillator cavity.

Plate 2

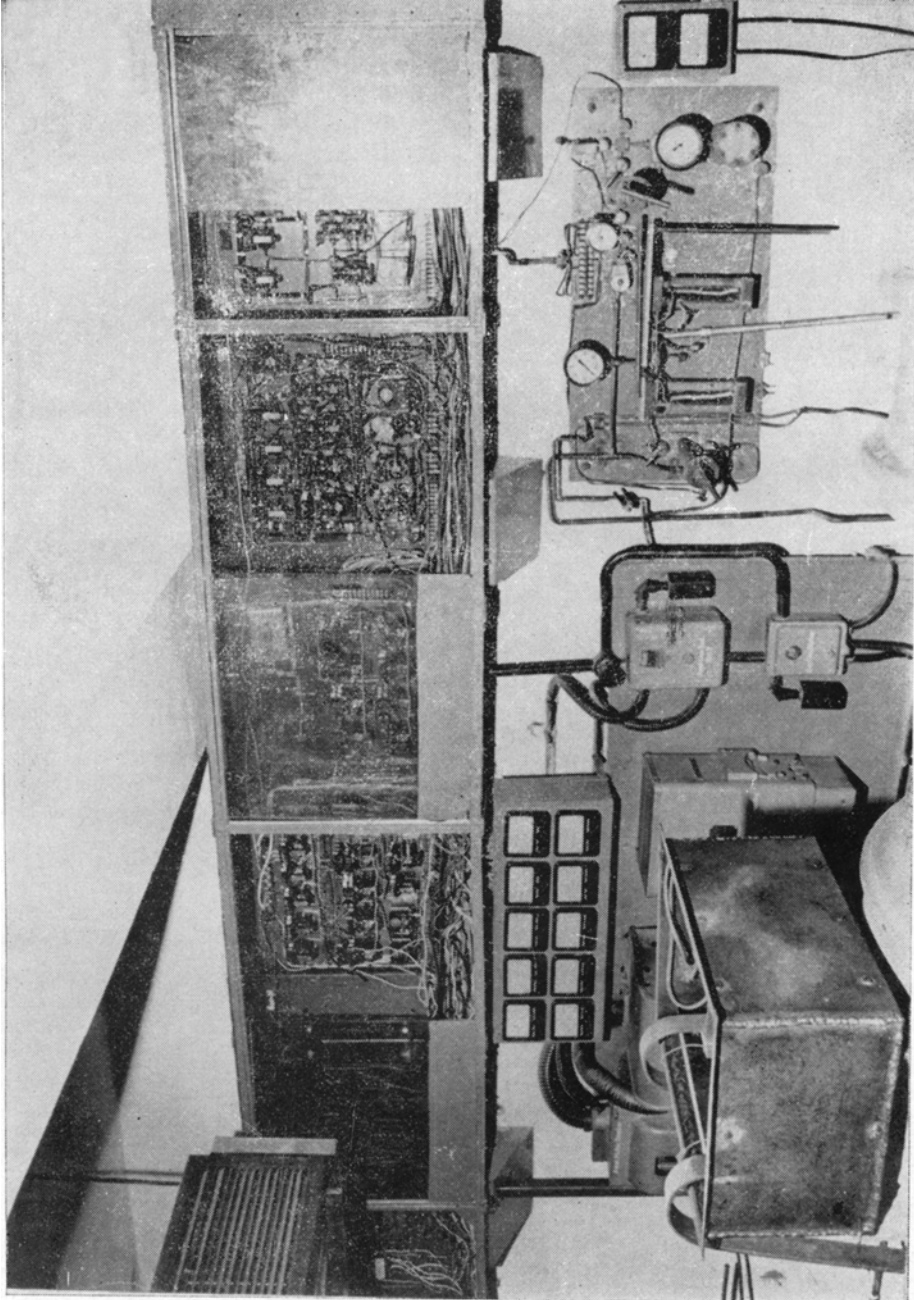


Figure 9. Relay system showing a part of the relay panel.